LANGMUIR

pubs.acs.org/Langmuir Article

Hierarchical Micro-Nanostructured Surfaces for Isotropic/Anisotropic Liquid Transport

Ramesh Shrestha, Bowen Yu, Qian Yang, Wei Gong, and Sheng Shen*

Cite This: *Langmuir* 2020, 36, 1569−1573 Read Online

ACCESS | Metrics & More | Article Recommendations | Supporting Information

ABSTRACT: The control of liquid transport using hierarchical micro-nanostructured surfaces is of significant interest for a broad range of applications, including thermal management, digital lab-on-chip, self-cleaning surfaces, antifogging, and water harvesting, among others. Although a variety of fabrication techniques can be utilized to produce micro/nanostructured patterns for controlling liquid transport, each sample usually needs to be patterned and developed separately, making the micro/nanofabrication process tedious and expensive. Here, based on scalable template stripping and chemical oxidation techniques, we demonstrate hierarchical micro-nanostructured surfaces for isotropic or anisotropic liquid transport. Furthermore, the overall structure is thin and flexible, making it ideal for applications where geometry and weight are constrained, such as aerospace, flexible, and wearable devices.

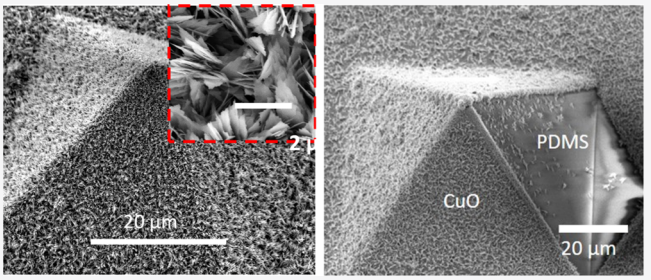

INTRODUCTION

Controlling liquid transport using hierarchical micro-nanostructured surfaces shows promise for a broad range of applications, including thermal management, self-cleaning surfaces, water harvesting, antifogging, and so forth.[1−4] To realize these applications, several fabrication techniques such as replica molding from natural surfaces,[5,6] colloidal assembly,[7] spinodal dewetting,[8] wrinkling,[9] and photolithography[2,10] have been implemented. As one of the most common fabrication techniques for micro/nanostructured surfaces, photolithography can readily produce micro/nanoscale patterns specifically designed for wetting applications. However, each sample generally needs to be patterned and developed individually with repeated processes, making the micro/nanofabrication process tedious and expensive. Here, based on scalable template stripping and chemical oxidation techniques, we demonstrate a thin and flexible hierarchical micro-nanostructured surface for liquid transport. Thin and flexible structures are highly desirable especially when weight and geometry concerns are significant in real applications such as aerospace, flexible, and wearable devices. The hierarchical micro-nanostructured surface developed in this work is not only superhydrophilic but also achieves high capillary performance in which the liquid spreading speed is maximized by optimizing geometric parameters.

Anisotropic liquid transport occurs when there exists asymmetry in surface energy,[11−13] Laplace pressure,[14−16] and/or pinning of liquid.[17] It has been achieved in several ways such as asymmetry in structures,[11] wettability,[18] or dynamic asymmetry using light,[19] temperature,[20] electric force,[21−23] and so forth. In this work, we also demonstrate that our fabrication process can be applied to develop asymmetric hierarchical surfaces for anisotropic liquid transport, where liquid spreads in a preferential direction.

EXPERIMENTAL SECTION

Fabrication of the Template with Inverted Pyramids. The template is made on a (100) silicon (Si) wafer with ∼300 nm silicon nitride (SiN_x) film. As the first step, an array of square holes is patterned on the SiN_x film using reactive ion etching. The patterned SiN_x layer serves as a mask layer for anisotropic KOH wet etching of the exposed area of the Si wafer. Thus, inverted pyramids are formed on the Si wafer, where the pyramidal size is controlled by the etching time. After etching Si, the SiN_x film is removed using hydrofluoric acid (HF).

Chemical Oxidation for Growing Copper Oxide (CuO) Nanostructures. A hot alkaline bath (∼95 °C) is prepared with a mixture of 3.5 g of sodium chlorite ($NaClO_2$), 5 g of sodium hydroxide (NaOH), 10 g of sodium phosphate dodecahydrate ($Na_3PO_4{\cdot}12H_2O$), and 100 mL of deionized (DI) water.[24,25] As the copper (Cu) micropyramid is immersed into the solution, the color immediately changes to black. The oxidation process leads to ∼2 μm tall blade-like sharp and dense nanostructures growing on the sample surface, which are mainly composed of CuO. Because of the self-limiting growth of the nanostructures, no discernible growth occurs after about 5 min.

Characterization of Isotropic and Anisotropic Liquid Spreading. The isotropic liquid spreading is characterized by measuring the rate of water rise along a sample in the vertical direction. The water rising process is recorded by a high-speed camera

Received: December 10, 2019
Revised: January 10, 2020
Published: January 23, 2020

https://dx.doi.org/10.1021/acs.langmuir.9b03800
Langmuir 2020, 36, 1569−1573

(Phantom v1211) at 500 frames/s. The anisotropic liquid spreading is demonstrated by recording the wicking waterfront of a DI water droplet on a sample using a charged coupled device (CCD) camera through a stereomicroscope at ~6 frames/s.

RESULTS AND DISCUSSION

In Figure 1a, we develop a wafer-scale technique to fabricate hierarchical micro-nanostructured surfaces by combining

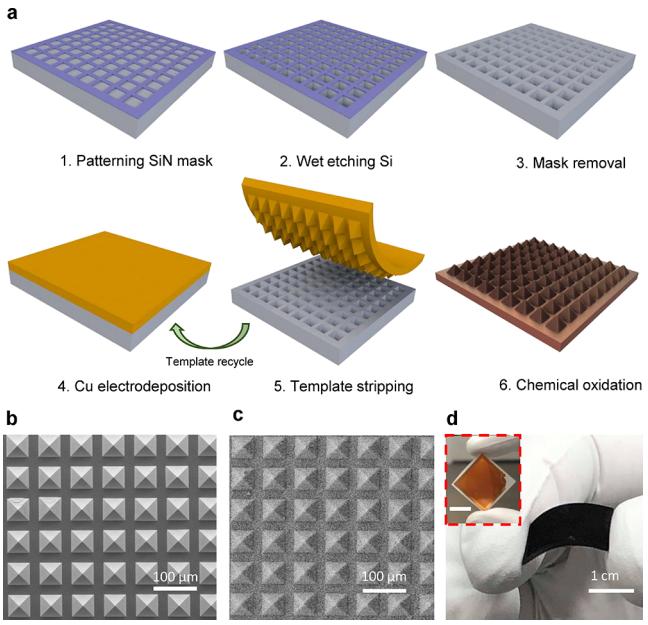

Figure 1. Fabrication of hierarchically rough surfaces for liquid transport. (a) Schematic of scalable template stripping technique to fabricate hierarchically rough Cu surfaces. (b) SEM image of Cu micropyramids. (c) SEM image of hierarchically-rough surface after chemical oxidation. (d) Photograph showing the flexibility of the samples. Inset is Cu micropyramid before oxidation. Upon oxidation, it appears black. Scale bar, 1 cm (inset in d).

template stripping[26,27] and chemical oxidation. The large-scale template used here is a bulk micromachined Si wafer on which inverted micropyramids are fabricated using wet etching. The Si template is then used to develop Cu micropyramidal structures by electrochemical deposition, where the inverted pyramids on the Si template are filled with Cu to form a continuous film. After electroplating, the deposited Cu film with replicated micropyramids is attached to a heat-release tape and can be easily peeled off in water at room temperature due to water-assisted debonding between Cu and the native oxide on the Si template.[28] The smooth and defect-free Cu micropyramid arrays are therefore fabricated as the base structure, as shown in Figures 1b,d inset for the stand-alone copper film. After chemical oxidation, the smooth Cu micropyramidal surface appears to be rough (Figure 1c), and its color turns from copper to black (Figure 1d) because CuO nanostructures are grown on the Cu surface upon oxidation (see the Supporting Information for X-ray analysis of the oxide surface).[29] Both the Cu micropyramidal and the oxidized samples show high flexibility (Figure 1d). The heat-release tape was detached from the sample due to high temperature of oxidation process. Because of sample flexibility, a new set of heat-release tape are used as rigid substrates for later experiment. Compared to previous liquid spreading surfaces,[10,15] the photolithography process conducted in this work is only required to fabricate the substrate or template, which can then be reused to produce multiple samples though electroplating and water-assisted peel off process.

The capillary or liquid spreading performance of a micro-nanostructured surface can be evaluated by the ratio of the permeability K and the effective pore size R_{eff}.[10] Here, R_{eff} is defined as $R_{eff} = r_p/\cos\theta$, where r_p is the pore radius and θ is the contact angle. In our structures, a larger pyramid size or gap between adjacent pyramids allows for a higher flow rate of the fluid, thus enhancing K; however, it simultaneously increases the pore radius (r_p) and therefore R_{eff}. Clearly, the pyramid size and gap need to be optimized to achieve a high K/R_{eff}. Moreover, to further enhance K/R_{eff}, we develop hierarchical micro-nanostructures by growing CuO nanostructures onto Cu micropyramids. With the fixed pyramid angle (54.7°) from the wet etching of Si, we study the liquid spreading behavior of the structures by varying pyramid size (L) and gap (P) (Figure 2a) (see Supporting Information

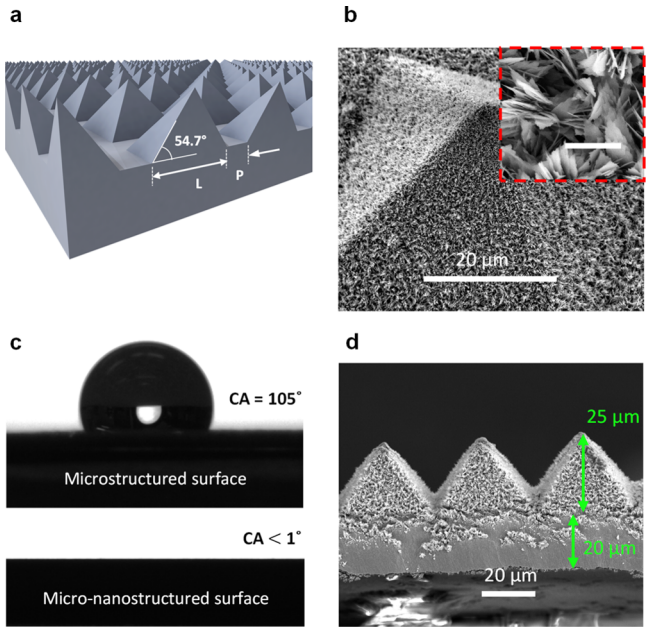

Figure 2. Optimization of Cu micropyramid geometry. (a) Schematic of Cu micropyramids. Pyramid side length (L) and gap (P) between two pyramids are tuned. (b) SEM images of typical oxidized Cu micropyramid structure showing hierarchical micro-nanostructures. Inset shows the blade-like nanostructures that grow uniformly over the surface upon oxidation. Scale bar 2 μm (inset of b). (c) Contact angle measurements on bare Cu micropyramids before oxidation and hierarchical micro-nanostructure after oxidation. (d) SEM image of the thinnest wick (~45 μm).

Table S1 for details). As shown in Figure 2b, ~2 μm long blade-like, dense CuO nanostructures are grown on the Cu micropyramids by chemical oxidation, where no discernible structure change occurs after 5 min due to the self-limiting growth of the nanostructures. Compared with the large contact angle (~105°) of a bare Cu micropyramidal surface in Figure 2c, the hierarchical micro-nanostructured surface turns out to be superhydrophilic with a contact angle of <1°. The overall sample thickness is as small as ~45 μm (Figure 2d).

We quantitatively characterize the liquid spreading performance of the hierarchical micro-nanostructured surfaces by measuring the rate of water rise along them in the vertical direction. In our experiment, a test sample is placed to be

https://dx.doi.org/10.1021/acs.langmuir.9b03800
Langmuir 2020, 36, 1569−1573

perpendicular to a water surface and moved slowly toward water using a high-resolution Z-manipulator. As soon as the sample touches the water surface, water quickly rises along the sample due to the high capillary pressure. The whole process is recorded by a high-speed camera (Phantom v1211) at 500 frames/s for front and side views of the sample subsequently, as shown in Figures 3a and S2. In Figure 3b schematic inset, a

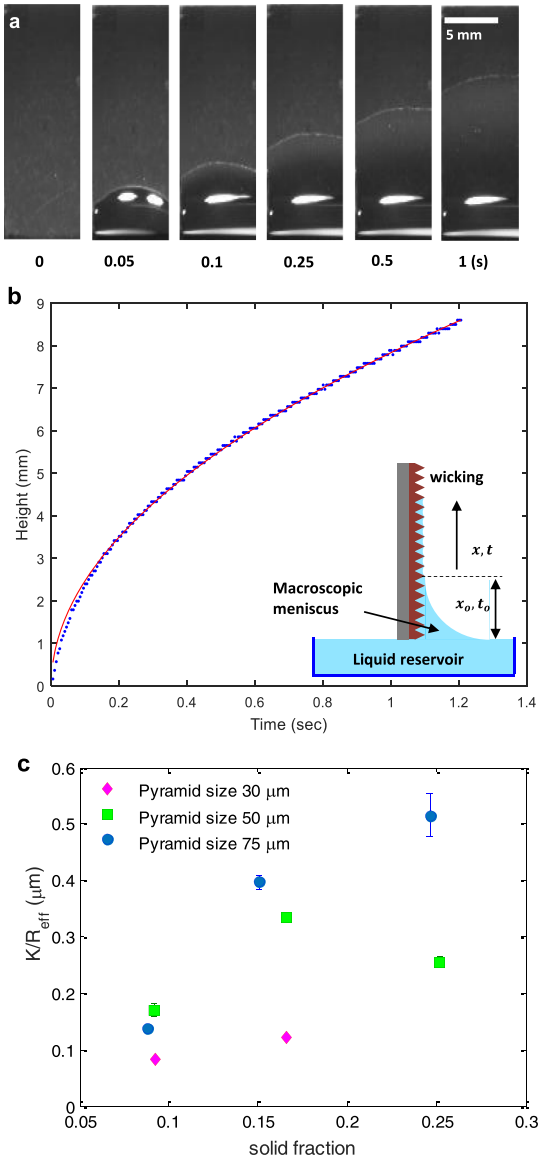

Figure 3. Characterization of the Cu-based micro-nanostructured wick. (a) Selected frames of the water rise measurement. (b) Capillary performance of a typical wick. Blue dots represent data obtained from image processing and red line represents the best curve fit using eq 1. The inserted schematic of the side view shows where the macroscale meniscus height and time are measured. (c) K/R_{eff} of all the samples. The error bar is based on standard error in curve fitting with 95% confidence interval.

macroscopic meniscus is first formed due to the balance between gravity and capillary force, and then water spreads through the micro-nanostructured pores. The maximum height of such macroscale meniscus is measured to be about 3.9 mm that is consistent with the predicted value (see Supporting Information). Since the gravity and the inertia effects are generally negligible for liquid spreading phenomena through micro/nanostructures, we use the Lucas−Washburn equation[10,30] as an approximation to describe the capillary behavior of our samples

$$x^2 = \left(\frac{2\sigma}{\varepsilon\mu}\right)\left(\frac{K}{R_{eff}}\right)t \quad (1)$$

where σ is the surface tension of water, μ is the dynamic viscosity of water, and ε, K, and R_{eff} are the porosity, permeability, and effective radius of the wick structure, respectively. Here, by approximating the hierarchical micro-nanostructure as a porous medium, the permeability K is defined as a property of the structure measuring its ability to transmit fluids. Although the Washburn equation cannot fully describe the complex flow inside the hierarchical micro-nanostructured surfaces in our work, it provides a good approximation for the macroscale waterfront travel behavior. More importantly, with the Washburn equation as an approximation, we have a common model for comparisons with other existing studies using hierarchical micro-nano-structured surfaces (see the Supporting Information).

It is worth noting that at the microscale, several waterfront lines rise distinctively and discontinuously through the sample structure while merging with their sideways. Although eq 1 describes the averaged macroscale behavior of waterfront travelling in a porous medium, it still provides a good approximation for capillary motion in the micropyramid-based wick. Using image processing in MATLAB, the waterfront is tracked and fitted with eq 1, as shown in Figure 3b. Based on the curve fitting and known liquid properties and wick parameters, K/R_{eff} values are extracted from eq 1. Figure 3c shows the K/R_{eff} values for all measured samples as a function of solid fraction $(1 - \varepsilon)$ (see the Supporting Information for estimation of the solid fraction), where the porosity (ε) is estimated assuming a flat meniscus. In reality, the meniscus has a finite curvature which reduces the cross-section area available for liquid transport.[10,31] Although both the pore radius and permeability increase with the decreasing solid fraction, the increase of the pore radius is faster than that of the permeability. Therefore, regardless of sizes, all of the samples show the decreasing K/R_{eff} as the solid fraction decreases. It is worth to note that this trend is different from the one in ref 10 because for the cylindrical shape structures, the permeability decreases faster than the effective pore radius, which results in an overall decreasing trend in K/R_{eff} with solid fraction.

Based on the results from isotropic wetting, we further control liquid transport in a preferential direction using the same fabrication technique for micropyramidal structures. Here, we introduce a surface energy gradient in each micropyramid by making one of its four side faces hydrophobic while leaving other three faces superhydrophilic. We utilize the same Si templates to fabricate asymmetric hierarchical micro-nanostructured surfaces for anisotropic liquid spreading. Instead of filling the inverted pyramids on the Si template with Cu in Figure 1a, we coat a polydimethylsiloxane (PDMS) film on the template and strip the film off after PDMS is cured. Then, we apply oblique angle electron beam (E-beam) evaporation to deposit a 50 nm thick gold (Au) film onto three faces of each PDMS micropyramid as a seed layer for electrochemical deposition. During the electroplating, only the areas covered with Au seed layers will grow Cu and subsequently be oxidized for developing the CuO nanostruc-

https://dx.doi.org/10.1021/acs.langmuir.9b03800
Langmuir 2020, 36, 1569−1573

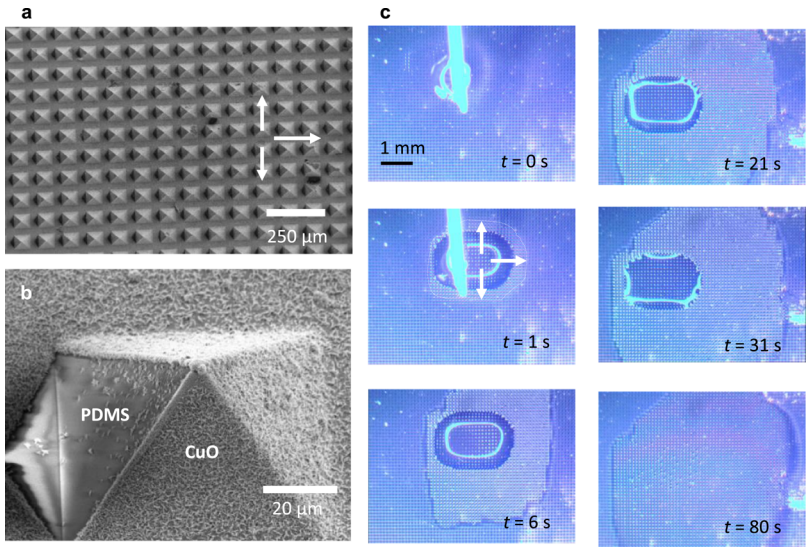

Figure 4. Preferential liquid spreading. (a) SEM image of asymmetric surface designed to make preferential liquid spreading. Arrows indicate preferential wick direction. (b) Magnified SEM image showing the asymmetric surface. Three sides of the pyramid are covered with CuO nanostructures whereas one side of the pyramid is PDMS. (c) Time stamp images showing preferential wicking of a water droplet on the wick surface. Dotted white lines indicate the propagating waterfront whereas three arrows show preferential wicking directions. The anisotropy ratio in left versus right directions is ∼8. Within 80 s, the macroscale droplet spreads into the micropyramid channel. Afterward, water evaporates quickly due to the thin film evaporation.

tures. Figure 4a,b show the scanning electron microscopy (SEM) images of the asymmetric hierarchical structures for preferential liquid spreading.

When water propagates through the asymmetric hierarchical structure (Figure 4b), it experiences a higher surface energy facing the PDMS side. Such a decrease in wettability leads to the loss of capillary pressure and thus causes water frontline pinned in the left direction. As a proof of concept, we demonstrate the anisotropic liquid spreading by dripping a DI water droplet on the sample surface and recording the wicking waterfront using a CCD camera through a stereomicroscope at ∼6 frames/s. In Figure 4c, it can be seen from the selected frames that the water droplet spreads with a similar speed in the three directions indicated by the white arrows; however, it is pinned to the left. As expected, the direction with exposed PDMS shows an 8× smaller spreading length as compared to the other three directions. It should also be noted that at t = 21 s, the frame is shifted to the right in order to keep the propagating waterfront within the field of view of the stereomicroscope. By about 80 s, the droplet completely spreads out into the pores (Figure 4c). This is followed by the quick evaporation of the water film along the micropyramids.

CONCLUSIONS

In summary, we demonstrate a scalable approach to fabricate hierarchical micro-nanostructured surfaces for isotropic or anisotropic liquid transport. To achieve a high capillary performance in isotropic liquid spreading, the Cu micropyramidal surface is coated with nanostructures using chemical oxidation. The hierarchical micro-nanostructures turn the barely wetting Cu surface into a super-hydrophilic one with an almost zero-degree contact angle. The capillary performance generally increases on increasing solid fraction or pyramid size. By introducing surface energy gradient along the hierarchical micro-nanostructured surface, we also demonstrate anisotropic liquid spreading. Furthermore, the overall structure is flexible and only ∼45 μm thick, making it ideal for applications in aerospace, portable, and wearable devices.

ASSOCIATED CONTENT

Supporting Information

The Supporting Information is available free of charge at https://pubs.acs.org/doi/10.1021/acs.langmuir.9b03800.

Details of solid fraction estimation, macroscopic meniscus height prediction, chemical composition of the oxide surface by X-ray diffraction, side view during capillary test, comparison of capillary performance with other literature values, and anisotropic liquid transport (PDF)

AUTHOR INFORMATION

Corresponding Author

Sheng Shen − *Department of Mechanical Engineering, Carnegie Mellon University (CMU), Pittsburgh, Pennsylvania 15213, United States;* orcid.org/0000-0002-9951-0814; Email: sshen1@cmu.edu

Authors

Ramesh Shrestha − *Department of Mechanical Engineering, Carnegie Mellon University (CMU), Pittsburgh, Pennsylvania 15213, United States*

Bowen Yu − *Department of Mechanical Engineering, Carnegie Mellon University (CMU), Pittsburgh, Pennsylvania 15213, United States*

Qian Yang − *Department of Mechanical Engineering, Carnegie Mellon University (CMU), Pittsburgh, Pennsylvania 15213, United States*

Wei Gong − *Department of Mechanical Engineering, Carnegie Mellon University (CMU), Pittsburgh, Pennsylvania 15213, United States*

Complete contact information is available at: https://pubs.acs.org/10.1021/acs.langmuir.9b03800

https://dx.doi.org/10.1021/acs.langmuir.9b03800
Langmuir 2020, 36, 1569−1573

Notes

The authors declare no competing financial interest.

■ ACKNOWLEDGMENTS

This work is supported by the National Science Foundation (CMMI-1916110). We would like to thank Prince Shival Singh (CMU) for helpful discussions on electrodeposition, Dr. Deepak Patil (Intel), Dr. Fred Higgs (Rice University) and Dr. Maarten P de. Boer (CMU) for helps with high speed camera.

■ REFERENCES

(1) Liu, K.; Yao, X.; Jiang, L. Recent Developments in Bio-Inspired Special Wettability. *Chem. Soc. Rev.* **2010**, *39*, 3240−3255.
(2) Launay, S.; Fedorov, A. G.; Joshi, Y.; Cao, A.; Ajayan, P. M. Hybrid Micro-Nano Structured Thermal Interfaces for Pool Boiling Heat Transfer Enhancement. *Microelectron. J.* **2006**, *37*, 1158−1164.
(3) Bhushan, B.; Jung, Y. C.; Koch, K. Micro-, Nano- and Hierarchical Structures for Superhydrophobicity, Self-Cleaning and Low Adhesion. *Philos. Trans.: Math., Phys. Eng. Sci.* **2009**, *367*, 1631−1672.
(4) Guo, P.; Zheng, Y.; Wen, M.; Song, C.; Lin, Y.; Jiang, L. Icephobic/Anti-Icing Properties of Micro/Nanostructured Surfaces. *Adv. Mater.* **2012**, *24*, 2642−2648.
(5) Lee, S.-M.; Kwon, T. H. Mass-Producible Replication of Highly Hydrophobic Surfaces from Plant Leaves. *Nanotechnology* **2006**, *17*, 3189−3196.
(6) Liu, B.; He, Y.; Fan, Y.; Wang, X. Fabricating Super-Hydrophobic Lotus-Leaf-Like Surfaces through Soft-Lithographic Imprinting. *Macromol. Rapid Commun.* **2006**, *27*, 1859−1864.
(7) Zhang, G.; Wang, D.; Gu, Z.-Z.; Möhwald, H. Fabrication of Superhydrophobic Surfaces from Binary Colloidal Assembly. *Langmuir* **2005**, *21*, 9143−9148.
(8) Higgins, A. M.; Jones, R. A. L. Anisotropic Spinodal Dewetting as a Route to Self-Assembly of Patterned Surfaces. *Nature* **2000**, *404*, 476−478.
(9) Lin, G.; Zhang, Q.; Lv, C.; Tang, Y.; Yin, J. Small Degree of Anisotropic Wetting on Self-Similar Hierarchical Wrinkled Surfaces. *Soft Matter* **2018**, *14*, 1517−1529.
(10) Nam, Y.; Sharratt, S.; Byon, C.; Kim, S. J.; Ju, Y. S. Fabrication and Characterization of the Capillary Performance of Super-hydrophilic Cu Micropost Arrays. *J. Microelectromech. Syst.* **2010**, *19*, 581−588.
(11) Chu, K.-H.; Xiao, R.; Wang, E. N. Uni-Directional Liquid Spreading on Asymmetric Nanostructured Surfaces. *Nat. Mater.* **2010**, *9*, 413−417.
(12) Bormashenko, E.; Bormashenko, Y.; Grynyov, R.; Aharoni, H.; Whyman, G.; Binks, B. P. Self-Propulsion of Liquid Marbles: Leidenfrost-Like Levitation Driven by Marangoni Flow. *J. Phys. Chem. C* **2015**, *119*, 9910−9915.
(13) Cira, N. J.; Benusiglio, A.; Prakash, M. Vapour-Mediated Sensing and Motility in Two-Component Droplets. *Nature* **2015**, *519*, 446−450.
(14) Prakash, M.; Quere, D.; Bush, J. W. M. Surface Tension Transport of Prey by Feeding Shorebirds: the Capillary Ratchet. *Science* **2008**, *320*, 931−934.
(15) Lorenceau, L.; Qur, D. Drops on a Conical Wire. *J. Fluid Mech.* **2004**, *510*, 29−45.
(16) Ju, J.; Bai, H.; Zheng, Y.; Zhao, T.; Fang, R.; Jiang, L. A Multi-Structural and Multi-Functional Integrated Fog Collection System in Cactus. *Nat. Commun.* **2012**, *3*, 1247.
(17) Chen, H.; Zhang, P.; Zhang, L.; Liu, H.; Jiang, Y.; Zhang, D.; Han, Z.; Jiang, L. Continuous Directional Water Transport on the Peristome Surface of Nepenthes Alata. *Nature* **2016**, *532*, 85−89.
(18) Daniel, S.; Chaudhury, M. K.; Chen, J. C. Fast Drop Movements Resulting from the Phase Change on a Gradient Surface. *Science* **2001**, *291*, 633−636.
(19) Ichimura, K.; Oh, S. K.; Nakagawa, M. Light-Driven Motion of Liquids on a Photoresponsive Surface. *Science* **2000**, *288*, 1624−1626.
(20) Brzoska, J. B.; Brochard-Wyart, F.; Rondelez, F. Motions of Droplets on Hydrophobic Model Surfaces Induced by Thermal Gradients. *Langmuir* **1993**, *9*, 2220−2224.
(21) Pollack, M. G.; Fair, R. B.; Shenderov, A. D. Electrowetting-Based Actuation of Liquid Droplets for Microfluidic Applications. *Appl. Phys. Lett.* **2000**, *77*, 1725−1726.
(22) Wang, Z.; Ci, L.; Chen, L.; Nayak, S.; Ajayan, P. M.; Koratkar, N. Polarity-Dependent Electrochemically Controlled Transport of Water through Carbon Nanotube Membranes. *Nano Lett.* **2007**, *7*, 697−702.
(23) McHale, G.; Brown, C. V.; Newton, M. I.; Wells, G. G.; Sampara, N. Dielectrowetting Driven Spreading of Droplets. *Phys. Rev. Lett.* **2011**, *107*, 186101.
(24) Nam, Y.; Ju, Y. S. *Comparative Study of Copper Oxidation Schemes and Their Effects on Surface Wettability*. ASME 2008 IMECE Conference, 2008, pp. 1833−1838.
(25) Miljkovic, N.; Enright, R.; Nam, Y.; Lopez, K.; Dou, N.; Sack, J.; Wang, E. N. Jumping-Droplet-Enhanced Condensation on Scalable Superhydrophobic Nanostructured Surfaces. *Nano Lett.* **2013**, *13*, 179−187.
(26) Li, P.; Liu, B.; Ni, Y.; Liew, K. K.; Sze, J.; Chen, S.; Shen, S. Large-Scale Nanophotonic Solar Selective Absorbers for High-Efficiency Solar Thermal Energy Conversion. *Adv. Mater.* **2015**, *27*, 4585−4591.
(27) Nagpal, P.; Lindquist, N. C.; Oh, S.-H.; Norris, D. J. Ultrasmooth Patterned Metals for Plasmonics and Metamaterials. *Science* **2009**, *325*, 594−597.
(28) Lee, C. H.; Kim, J. H.; Zou, C.; Cho, I. S.; Weisse, J. M.; Nemeth, W.; Wang, Q.; van Duin, A. C. T.; Kim, T. S.; Zheng, X. Peel-and-Stick: Mechanism Study for Efficient Fabrication of Flexible/Transparent Thin-Film Electronics. *Sci. Rep.* **2013**, *3*, 2917.
(29) Nam, Y.; Ju, Y. S. A Comparative Study of the Morphology and Wetting Characteristics of Micro/Nanostructured Cu Surfaces for Phase Change Heat Transfer Applications. *J. Adhes. Sci. Technol.* **2013**, *27*, 2163−2176.
(30) Washburn, E. W. The Dynamics of Capillary Flow. *Phys. Rev.* **1921**, *17*, 273−283.
(31) Byon, C.; Kim, S. J. The Effect of Meniscus on the Permeability of Micro-Post Arrays. *J. Micromech. Microeng.* **2011**, *21*, 115011.

https://dx.doi.org/10.1021/acs.langmuir.9b03800
Langmuir 2020, 36, 1569−1573